American Mineralogist, Volume 92, pages 1492–1501, 2007

The crystal structure of pyroxenes along the jadeite–hedenbergite and jadeite–aegirine joins

F. Nestola,[1,*] M. Tribaudino,[2] T. Boffa Ballaran,[1] C. Liebske,[3] and M. Bruno[4]

[1]Bayerisches Geoinstitut, Universität Bayreuth, Universitätstrasse 37, D-95447, Bayreuth, Germany
[2]Dipartimento di Scienze della Terra, Università di Parma, Parco Area delle Scienze 157/A, I-43100, Parma, Italy
[3]Institute for Mineralogy and Petrology, ETH Zurich, Clausiusstrasse 25, CH-8092, Zurich, Switzerland
[4]Dipartimento di Scienze Mineralogiche e Petrologiche, Università di Torino, Via Valperga Caluso 35, I-10125, Torino, Italy

Abstract

The crystal-structures of seven synthetic pyroxenes along the jadeite–hedenbergite ($Jd_{57}Hd_{43}$, $Jd_{26}Hd_{74}$, Jd_0Hd_{100}) and jadeite–aegirine ($Jd_{100}Ae_0$, $Jd_{76}Ae_{24}$, $Jd_{35}Ae_{65}$, Jd_0Ae_{100}) joins were refined using data collected by means of single-crystal X-ray diffraction (space group $C2/c$, $R_{4\sigma}$ between 2.2 and 3.4%).

The M2 and M1 polyhedral volumes and bond lengths increase with increasing aegirine and hedenbergite content, moreover the Ca for Na substitution along the jadeite–hedenbergite join changes the M2 coordination from 6 + 2 to 4 + 4, with remarkable tilting of the tetrahedral chains. The value of the displacement parameters follows the trend $U_{eq}M2 > U_{eq}O2 > U_{eq}O3 > U_{eq}O1 > U_{eq}M1 \approx U_{eq}T$ for all samples belonging to the jadeite–aegirine join and for pure hedenbergite; in contrast,, for pyroxenes with intermediate compositions between hedenbergite and jadeite the trend is $U_{eq}O1 > U_{eq}O2 > U_{eq}M2 > U_{eq}O3 > U_{eq}M1 \approx U_{eq}T$, with O1 and O2 having anomalously large displacement parameters, probably due to different local structural configuration around the cations with different size and charge.

Cation substitution at the M1 site of Na-pyroxenes gives rise to a different structural deformation with respect of the double substitution at both the M1 and M2 sites in $(Na,Ca)(M^{3+},M^{2+})Si_2O_6$ pyroxenes as the rigid tetrahedral chains try to accommodate both the increasing size of the M1 site and the different coordination requirement of the M2 site.

Keywords: Single crystal, X-ray diffraction, crystal-structure, clinopyroxenes

Introduction

Pyroxenes are among the most common minerals in the crust and the upper mantle and are major constituents in several meteorites; knowledge of their structural and thermodynamic properties is hence important in petrological modeling. In particular, Na-bearing pyroxenes are key phases in high-pressure and extreme pressure assemblages, up to more than 20 GPa and 1600 °C (Tutti et al. 2000). Natural Na-bearing pyroxenes are solid solutions of jadeite (Jd, $NaAlSi_2O_6$) with aegirine (Ae, $NaFe^{3+}Si_2O_6$), diopside (Di, $CaMgSi_2O_6$), and hedenbergite (Hd, $CaFe^{2+}Si_2O_6$). The end-members display $C2/c$ space group, whereas natural omphacitic pyroxenes in eclogitic assemblages, with a composition close to the binary jadeite–diopside join, display a transformation from $C2/c$ to $P2/n$ at intermediate compositions, related to coupled Ca/Na and Al/Mg cation ordering. Several structural and crystal chemical investigations were performed on the binary solid solutions of aegirine–jadeite and diopside–jadeite (e.g., Popp and Gilbert 1972; Carpenter et al. 1990a, 1990b; Holland 1983; Gasparik 1985; Boffa Ballaran et al. 1998). However, very few studies are available on pyroxenes along the aegirine–hedenbergite, jadeite–hedenbergite, and jadeite–aegirine joins. Structural data obtained from single-crystal X-ray diffraction are limited to the end-members (Cameron et al. 1973; Rossi et al. 1983; Boffa Ballaran et al. 1998; Heuer et al. 2005; Redhammer et al. 2000), whereas refinements of both single-crystal and powder data are available for several synthetic pyroxenes along the aegirine–hedenbergite join (Redhammer et al. 2000, 2006). For the aegirine–jadeite solid solution only unit-cell parameters are reported (Liu and Bohlen 1995; Nestola et al. 2006).

Direct information on samples with mixed compositions instead of just a mere comparison between the end-members has the following advantages: (1) Cation substitution seldom occurs with fully ideal behavior. Clustering of likely cations and order-disorder behavior may occur in intermediate samples, affecting structural and thermodynamic properties. Local structural behavior at a short-range scale is averaged in single structure investigation, but may be revealed by the presence of anomalous atomic displacement parameters in the average structure for intermediate compositions (e.g., Tribaudino and Nestola 2002). (2) The structural analysis along a given join clarifies the mechanism of cation substitution. Moreover, subtle structural changes, which could be overlooked analyzing only the end-members, can be enhanced by the analysis of high quality structural data for intermediate compositions.

* Present address: Dipartimento di Geoscienze, Università di Padova, Corso Garibaldi 37, I-35137, Padova, Italy. E-mail: fabrizio.nestola@unipd.it

0003-004X/07/0809–1492$05.00/DOI: 10.2138/am.2007.2540

The structure of seven synthetic pyroxenes along the jadeite–aegirine and hedenbergite–jadeite joins was studied, to clarify the structural changes occurring for the isovalent substitution of Fe^{3+} for Al along the jadeite–aegirine join and for the coupled heterovalent substitution of $CaFe^{2+}$ for NaAl along the jadeite–hedenbergite join. The major aim is to outline a generalized mechanism of structural deformation for pyroxenes with cation substitutions at both the M1 and M2 sites.

This work is a part of a wider investigation on structural, compressional and thermal properties for pyroxenes belonging to jadeite–aegirine and jadeite–hedenbergite solid solutions.

Experimental methods

Single crystals along the Jd–Ae and Jd–Hd joins were synthesized using multianvil presses at the Bayerisches Geoinstitut Bayreuth and at the ETH Zürich. Synthesis experiments were carried out at a pressure of 6 GPa, at temperatures between 1300 and 1400 °C and with run times of 5–8 h. Initial starting materials were stoichiometric mixtures of oxides and salts ($CaCO_3$, SiO_2, Na_2SiO_3, Fe_2O_3, Al_2O_3), subsequently melted between 1200 and 1300 °C and then quenched to glasses. For the jadeite–hedenbergite compositions it was also necessary to reduce the Fe^{3+} of the glasses starting materials to Fe^{2+}, therefore, these were annealed for 24 h at 600 °C in a controlled atmosphere (CO_2/H_2). Details relative to the synthesis and compositions of the crystals along the jadeite–aegirine join are reported by Nestola et al. (2006). The microprobe analyses for the samples along the jadeite–hedenbergite join are reported in Table 1a. For these three pyroxenes the analyses were performed at the "Istituto di Geoscienze e Georisorse," CNR Padova (Italy) using a CAMECA-CAMEBAX electron microprobe operating with a fine-focused beam (~1 μm) at an acceleration voltage of 15 kV and a beam current of 15 nA in wave-length dispersive mode (WDS), with 20 s counting times for both peak and total background. The following standards were used: $NaAlSi_3O_8$ for Na, MgO for Mg, Al_2O_3 for Al, $CaSiO_3$ for Si and Ca, and Fe_2O_3 for Fe.

Intensity data were collected using a Kappa geometry Xcalibur diffractometer with graphite monochromated Mo*K*α radiation ($5 \le 2\theta \le 80°$) in an ω-scan mode with a continuous-integrative step scan (0.05°/s, 60 scan steps, scan width 1.2°) under ambient conditions. The sample-detector distance was 135 mm. The program Win-IntegrStp (version 3.3, Angel 2003) was used to integrate the step-scan data applying the Lorentz-polarization correction. The intensity data were corrected for absorption using the program ABSORB V6.0 (Angel 2004). Weighted structural anisotropic refinements were done using the SHELX-97 package (Sheldrick 1997) starting from the atomic coordinates of Cameron et al. (1973). The atomic scattering curves were taken from the International Table for X-ray Crystallography (Ibers and Hamilton 1974). Ionized scattering factors were used for the cations at the M1 and M2 sites, whereas neutral vs. ionized scattering factors were used for the oxygen and Si atoms. Final occupancies were obtained following the same refinement procedure used in several works on cation partitioning of Na-clinopyroxenes (Rossi et al. 1983; Oberti and Caporuscio 1991; Boffa Ballaran et al. 1998). During the refinement of the hedenbergite sample a residual of 1.72 $e^-/Å^3$ in the difference Fourier map suggested the presence of a M2' split position occupied by Fe^{2+} as observed in previous studies (Bruno et al. 1982; Rossi et al. 1987; Oberti and Caporuscio 1991; Boffa Ballaran et al. 1998; Tribaudino and Nestola 2002; Nestola and Tribaudino 2003). Further refinements were, therefore, performed with an isotropic M2' position and with the constraint Ca (M2) + Fe^{2+} (M2') = 1.

Cation occupancies obtained by crystal structure refinement for all samples are reported in Table 1b. Unit-cell parameters, data collection and refinement details, fractional atomic coordinates, anisotropic thermal parameters, and polyhedral bond lengths and volumes are reported in Tables 2, 3, and 4, respectively.

Table 1a. Electron-microprobe analysis of the same crystals used for the single-crystal investigation (oxides in % by weight) for the samples along the Jd–Hd join

Nom. Comp.	$Jd_{50}Hd_{50}$	$Jd_{25}Hd_{75}$	Jd_0Hd_{100}
SiO_2	53.2(2)	50.0(3)	48.2(2)
Al_2O_3	12.3(2)	5.8(2)	0.22(6)
FeO	15.8(2)	23.2(4)	28.6(3)
Na_2O	7.2(2)	3.02(7)	0.03(2)
CaO	11.6(2)	17.6(2)	22.3(3)
MgO	–	0.08(6)	0.19(4)
Total	100.1	99.7	99.4
No. analyses	7	9	9

Table 1b. Cation partitioning obtained from crystal-structure refinements

	$Jd_{100}Ae_0$	$Jd_{74}Ae_{26}$	$Jd_{35}Ae_{65}$	Jd_0Ae_{100}	$Jd_{53}Hd_{47}$	$Jd_{24}Hd_{76}$	Jd_0Hd_{100}
T site							
Si	2.00(1)	2.00(1)	2.00(1)	2.00(1)	2.00(1)	2.00(1)	2.00(1)
M1 site							
^{VI}Al	1.00(1)	0.74(1)	0.35(1)	–	0.52(1)	0.24(1)	
Fe^{2+}	–	–	–	–	0.48(1)	0.76(1)	1.00(1)
Fe^{3+}	–	0.26(1)	0.65(1)	1.00(1)	–	–	–
Mg	–	–	–	–			
M2 site							
Na	1.00(1)	–	1.00(1)	1.00(1)	0.53(1)	0.24(1)	–
Ca	–	–	–	–	0.47(1)	0.76(1)	0.99(1)
M2′ site							
Fe^{2+}	–	–	–	–	0.03(1)	–	0.01(1)
Total	4.00	4.00	4.00	4.00	4.00	4.00	4.00

Results

Unit-cell parameters

The unit-cell parameters along the jadeite–aegirine and jadeite–hedenbergite joins are shown in Figure 1 as a function of composition. In both systems, a decrease in jadeite component leads to a non-linear increase of the *a* and *b* cell parameters (Figs. 1a and 1b). The *c* parameter (Fig. 1c) increases linearly along the jadeite–aegirine, although the absolute increase is not as pronounced as that of *a* and *b*. Along the jadeite–hedenbergite join the *c* parameter has a strong deviation from linearity with samples at intermediate compositions having larger values than the end-members (Fig. 1c). The β angle is constant along the jadeite–aegirine join, while it decreases non-linearly along the jadeite–hedenbergite join (Fig. 1d). As a result, the unit-cell volume increases significantly for both joins (Fig. 1e). The volume-composition trend is not linear for both the solid solutions, (see also Nestola et al. 2006), suggesting that some non-ideality also is associated with Al/Fe^{3+} substitution in contrast with previous results (Liu and Bohlen 1995). We also show in Figure 1e the linear trends between the end-members to better emphasize the small but significant deviation from linearity.

M2 polyhedron

The M2 cation is surrounded by two O1s, two O2s, and four O3s. In the following discussion we refer to M2 as "coordinated" with all of these O atoms, whether or not actual bonds exist. The volume of the M2 polyhedron increases non-linearly from jadeite to both aegirine and hedenbergite, which have similar M2 volumes within one standard deviation (Fig. 2a). The behavior of this site seems, therefore, unrelated to the size of the occupying cation: in fact, along jadeite–aegirine Na is the only cation at the M2 site, whereas along jadeite–hedenbergite the substitution of Ca whose cation radius in eightfold coordination is slightly smaller than that of Na (1.12 vs. 1.18 Å, Shannon 1976) gives rise to M2 volumes larger than those along the jadeite–aegirine solid solution. The M2 volume variations depend, hence, mainly on the cation substitutions at the M1 site: the M2 polyhedron is a relatively "soft" unit and its volume and shape are largely affected by changes of the M1 and T polyhedra (Thompson and Downs 2004). The M2-O1, M2-O2, and M2-$O3_{(short)}$ bond lengths change in a similar way along the two joins (Figs. 2b and 2c): the M2-O1 bond length is nearly constant, the M2-O2

TABLE 2. Unit-cell parameters and crystal-structure refinement details

Samples	$Jd_{100}Ae_0$*	$Jd_{74}Ae_{26}$*	$Jd_{35}Ae_{65}$*	Jd_0Ae_{100}*	$Jd_{53}Hd_{47}$	$Jd_{24}Hd_{76}$	Jd_0Hd_{100}
a (Å)	9.4278(3)	9.4781(2)	9.5663(2)	9.6623(4)	9.6031(3)	9.7340(2)	9.8447(2)
b (Å)	8.5651(4)	8.6180(3)	8.7040(3)	8.8000(2)	8.7735(3)	8.9103(4)	9.0234(3)
c (Å)	5.2262(2)	5.2449(2)	5.2733(2)	5.2956(4)	5.2656(2)	5.2682(2)	5.2509(2)
β (°)	107.624(2)	107.570(2)	107.600(2)	107.579(3)	106.725(3)	105.904(2)	104.862(2)
V (Å^3)	402.21(2)	408.43(2)	418.54(2)	429.25(3)	424.88(2)	439.44(3)	450.84(2)
Space group	*C*2/*c*	*C*2/*c*	*C*2/*c*	*C*2/*c*	*C*2/*c*	*C*2/*c*	*C*2/*c*
Z	4	4	4	4	4	4	4
Radiation	Mo*K*α	Mo*K*α	Mo*K*α	Mo*K*α	Mo*K*α	Mo*K*α	Mo*K*α
Crystal size (μm^3)	140 × 48 × 35	140 × 95 × 50	140 × 70 × 55	180 × 90 × 55	120 × 85 × 60	150 × 70 × 40	130 × 90 × 55
Scan type	ω scan	ω scan	ω scan	ω scan	ω scan	ω scan	ω scan
Absorption correction	ABSORB V6.0†	ABSORB V6.0	ABSORB V6.0	ABSORB V6.0	ABSORB V6.0	ABSORB V6.0	ABSORB V6.0
No. of indep. refl. $I > 4\sigma$	932	969	968	968	880	929	1099
θ_{max} (°)	40.00	40.00	40.00	40.00	40.00	40.00	40.00
R_1 (F) (%)	3.20	2.83	2.18	2.83	3.42	3.40	2.99
No. parameters	48	50	50	48	54	52	54
GooF	0.90	1.07	1.12	1.00	0.87	0.99	1.05

* These samples are the same studied by Nestola et al. (2006).
† Angel (2004).

decreases; and the M2-$O3_{(short)}$ increases with increasing aegirine and hedenbergite content. The M2-$O3_{(long)}$ distance instead increases significantly with increasing aegirine and decreases with increasing hedenbergite component (Fig. 2d). The ΔM2 distortion parameter (Dal Negro et al. 1982), expressed as ΔM2 = M2-$O3_{(long)}$ – [M2-O1 + M2-O2 + M2-$O3_{(short)}$]/3, increases with aegirine and decreases with hedenbergite component (Fig. 2e). The ΔM2 distortion parameter describes how the coordination of the M2 site deviates from an eightfold coordination. In hedenbergite, whose ΔM2 parameter is the smallest, the M2-O2 and M2-O1 distances are markedly different with respect to the M2-$O3_{(short)}$ and M2-$O3_{(long)}$ distances, and the coordination is better described as 4 + 4 leading to an eightfold coordination around the M2 site. In jadeite and even more pronounced in aegirine, the two M2-$O3_{(long)}$ bonds are much larger than the other M2-O bond distances and the coordination can be better described as a 6 + 2. The change from the 6 + 2 to a 4 + 4 coordination of the M2 site (involving the two O3 sites) between Na and Ca pyroxenes is in agreement with previous data on aegirine and hedenbergite (Redhammer et al. 2000, 2006).

M1 octahedron

The M1 polyhedral volume (Fig. 3a) and the individual M1-O bond lengths (Figs. 3b and 3c) increase with increasing Fe^{3+} and Fe^{2+} substitutions at the M1 site in the jadeite–aegirine and jadeite–hedenbergite joins. However, while the bond lengths follow an almost linear trend along both joins, the polyhedral volumes show a non-linear behavior with a larger variation along the jadeite–hedenbergite solid solution. With increasing aegirine content, the absolute difference among the individual bond lengths is nearly unchanged (Fig. 3b), whereas it decreases with increasing hedenbergite content (Fig. 3c). The average <M1-O> bond lengths for both systems follow the same linear trend with the M1 cation size (Fig. 3d). The M1-M1 distance between adjacent M1 sites in the octahedral chains increases linearly along the jadeite–aegirine join, but shows a positive deviation from linearity along the jadeite–hedenbergite join (Fig. 3e). The M1-M1-M1 angle decreases almost linearly with increasing the aegirine content, and shows a negative deviation from linearity with increasing hedenbergite component (Fig. 3f). The same structural parameters also show the same non-linear behavior along the aegirine–hedenbergite join (Redhammer et al. 2000).

T tetrahedron

Along the jadeite–aegirine join the tetrahedral bond lengths show a continuous, but rather small change between the two end-members (Fig. 4a). In detail, there is a crossover between the T-O1, which is longer in jadeite, and the T-$O3_{(short)}$ distance at a composition of about $Jd_{60}Ae_{40}$. The T-O2 bond is significantly shorter than the others along the whole join, and the other T-O bonds have similar values, as commonly observed in Na pyroxenes. Along the jadeite–hedenbergite join, the values of T-O bond lengths between bridging O3 and non-bridging O1 and O2 atoms become clearly different with increasing hedenbergite content (Fig. 4b), with the T-O1 distance approaching the T-O2 value. The configuration in hedenbergite is commonly observed in pyroxenes with divalent cations at both M2 and M1 sites.

The tetrahedral volume (Fig. 4c), which increases slightly with increasing aegirine content, shows a more pronounced increase a function of hedenbergite substitution. The same behavior is observed for the average T-O bond distances (Fig. 4d). The O3-O3-O3 and T-O-T angles, related to the kinking of the tetrahedral chains, decrease continuously along the jadeite–hedenbergite join, whereas they are practically constant along the jadeite–aegirine join (Figs. 4e and 4f).

Displacement parameters

The equivalent displacement parameters U_{eq} (Table 3) show a different trend for the two joins. Along the jadeite–aegirine join the displacement parameters do not change significantly and follow for all compositions the pattern $U_{eq}(M2) > U_{eq}(O2) > U_{eq}(O3) > U_{eq}(O1) > U_{eq}(M1) \approx U_{eq}(T)$ (Figs. 5a and 5b), as commonly observed for end-member pyroxenes (Cameron et al. 1973). As expected, the same pattern is observed for pure hedenbergite. For intermediate compositions along the jadeite–hedenbergite join the displacement parameters are significantly larger than those of the end-members (Figs. 5c and 5d) and the order scheme becomes $U_{eq}(O1) > U_{eq}(O2) > U_{eq}(M2) > U_{eq}(O3) > U_{eq}(M1) \approx U_{eq}(T)$ with $U_{eq}(O1)$ and $U_{eq}(O2)$ showing an anomalously larger value with respect to those of all the pyroxenes investigated in this work.

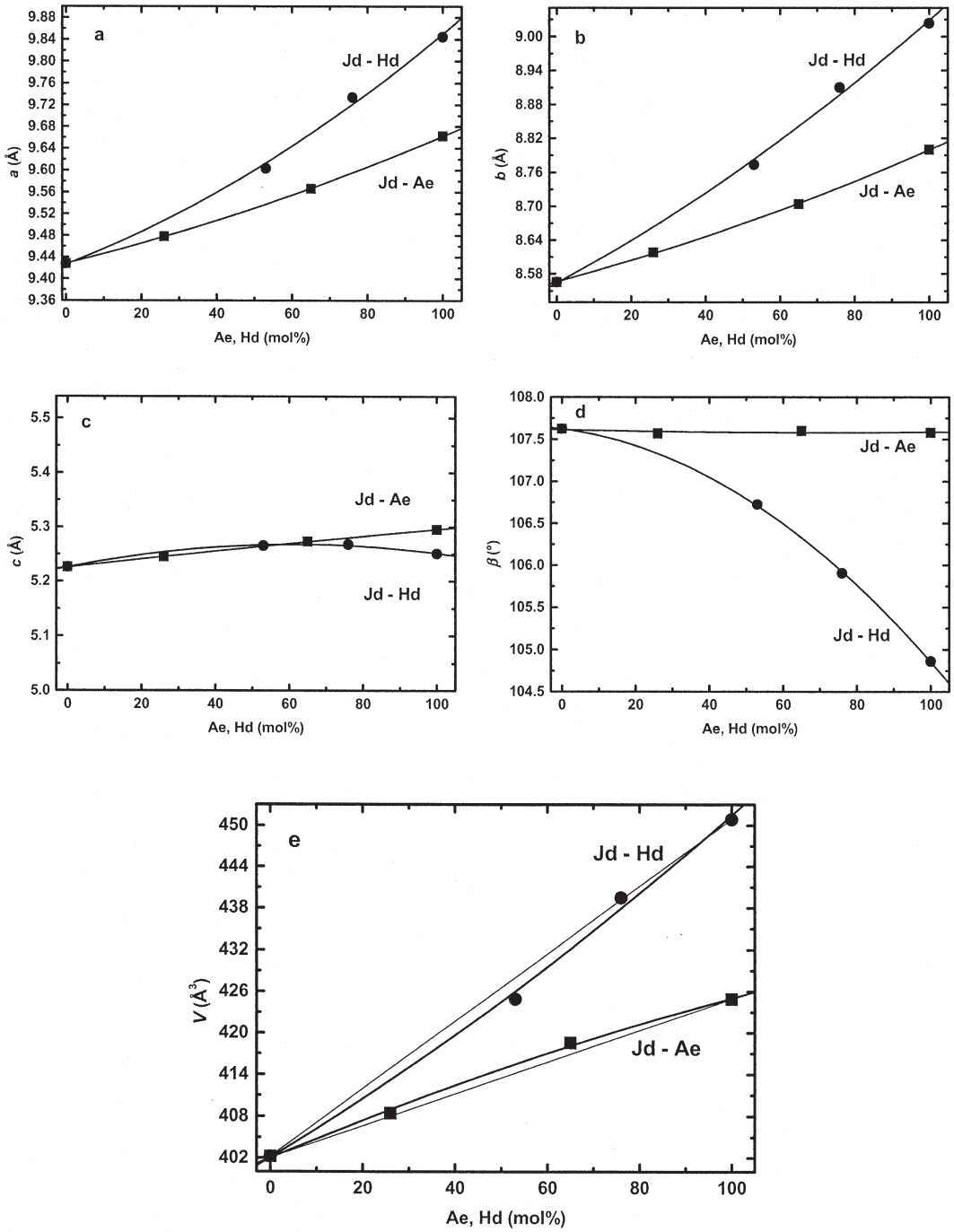

FIGURE 1. Unit-cell parameters and volumes along the jadeite–hedenbergite and jadeite–aegirine joins investigated in the present work. Squares = jadeite–aegirine join; circles = jadeite–hedenbergite join. The symbols used are larger than 1σ.

DISCUSSION

Structural deformations of Na-Ca pyroxenes

Cation substitution affects the unit-cell parameters of pyroxenes with different composition and gives rise to an overall macroscopic compositional strain with respect to pure pyroxene end-members. The corresponding strain tensor may be calculated from the cell parameters of samples with different composition and is geometrically represented by a triaxial ellipsoid, whose axes are the diagonal components of the strain tensor (Ohashi and Burnham 1973). In monoclinic pyroxenes, the strain ellipsoid is constrained by symmetry to have two axes lying in the (010) plane and the third coinciding with the **b** axis. The relevant variables are the size of the axes and their orientation in the (010) plane with respect to the crystallographic **a** and **c** directions. To assess the deformation induced by NaAl-$CaFe^{2+}$ and Al-Fe^{3+}

TABLE 3. Fractional atomic coordinates and anisotropic displacement parameters

Samples		$Jd_{100}Ae_0$	$Jd_{74}Ae_{26}$	$Jd_{35}Ae_{65}$	Jd_0Ae_{100}	$Jd_{53}Hd_{47}$	$Jd_{24}Hde_{76}$	Jd_0Hd_{100}
M2	x	0	0	0	0	0	0	0
	y	0.3002(1)	0.30029(7)	0.29844(8)	0.2961(1)	0.30094(8)	0.30061(8)	0.30034(5)
	z	0.25	0.25	0.25	0.25	0.25	0.25	0.25
	U_{11}	0.0146(4)	0.0143(3)	0.0140(3)	0.0131(5)	0.0165(3)	0.0137(3)	0.0104(2)
	U_{22}	0.0075(3)	0.0076(2)	0.0095(3)	0.0114(5)	0.0093(2)	0.0090(3)	0.0073(2)
	U_{33}	0.0090(3)	0.0094(2)	0.0086(3)	0.0062(4)	0.0090(3)	0.0092(3)	0.0073(2)
	U_{12}	0	0	0	0	0	0	0
	U_{13}	–0.0006(3)	–0.0008(2)	–0.0014(2)	–0.0027(4)	–0.0001(2)	–0.0005(2)	0.0001(1)
	U_{23}	0	0	0	0.0000	0	0	0
	U_{eq}	0.0108(2)	0.0114(1)	0.0118(2)	0.0115(2)	0.0124(2)	0.0114(3)	0.00873(9)
M2′	x	–	–	–	–	0	–	0
	y	–	–	–	–	0.257(7)	–	0.242(5)
	z	–	–	–	–	0.25	–	0.25
	U_{iso}	–	–	–	–	0.007(2)	–	0.0065(9)
M1	x	0	0	0	0	0	0	0
	y	0.90604(7)	0.90369(3)	0.90134(3)	0.89921(4)	0.90504(5)	0.90603(5)	0.90741(3)
	z	0.25	0.25	0.25	0.25	0.25	0.25	0.25
	U_{11}	0.0048(2)	0.0050(1)	0.0053(1)	0.0051(1)	0.0075(2)	0.0074(2)	0.0067(1)
	U_{22}	0.0044(2)	0.0047(1)	0.0053(1)	0.0045(2)	0.0080(2)	0.0073(2)	0.0058(1)
	U_{33}	0.0042(2)	0.0050(1)	0.0054(1)	0.0051(2)	0.0065(2)	0.0071(2)	0.0063(1)
	U_{12}	0	0	0	0	0	0	0
	U_{13}	0.0012(2)	0.0012(1)	0.00117(8)	0.0004(1)	0.0019(1)	0.0009(1)	0.0011(1)
	U_{23}	0	0	0	0	0	0	0
	U_{eq}	0.0043(1)	0.00494(9)	0.00542(7)	0.52(1)	0.0074(1)	0.0075(1)	0.00635(7)
T	x	0.29072(4)	0.29055(3)	0.29075(3)	0.29114(6)	0.28845(5)	0.28782(6)	0.28786(5)
	y	0.09342(4)	0.09232(3)	0.09083(3)	0.08943(5)	0.09209(5)	0.09199(6)	0.09244(4)
	z	0.22822(8)	0.22978(5)	0.23362(6)	0.23775(10)	0.22982(8)	0.2317(1)	0.23259(9)
	U_{11}	0.0039(2)	0.0042(1)	0.0046(1)	0.0046(2)	0.0068(2)	0.0064(2)	0.0050(2)
	U_{22}	0.0040(2)	0.0046(1)	0.0053(1)	0.0048(2)	0.0077(2)	0.0082(2)	0.0052(2)
	U_{33}	0.0041(2)	0.0045(1)	0.0051(1)	0.0053(1)	0.0056(2)	0.0060(2)	0.0048(2)
	U_{12}	–0.0003(1)	–0.00024(7)	–0.00007(8)	–0.0005(1)	0.0003(2)	0.0002(2)	–0.0002(1)
	U_{13}	0.0010(1)	0.00125(8)	0.00150(9)	–0.0006(2)	0.0025(2)	0.0017(2)	0.0012(1)
	U_{23}	–0.0004(1)	–0.00023(6)	–0.00021(8)	–0.0002(1)	–0.0011(2)	–0.0006(2)	–0.0004(1)
	U_{eq}	0.00383(9)	0.00443(7)	0.00500(7)	0.0051(1)	0.0066(1)	0.0069(1)	0.0050(1)
O1	x	0.1092(1)	0.11032(8)	0.11233(9)	0.1147(2)	0.1126(1)	0.1165(2)	0.1194(1)
	y	0.0760(1)	0.07663(8)	0.07785(9)	0.0789(2)	0.0808(1)	0.0853(2)	0.0901(1)
	z	0.1284(2)	0.1303(1)	0.1345(2)	0.1392(3)	0.1366(3)	0.1451(3)	0.1519(2)
	U_{11}	0.0043(3)	0.0046(3)	0.0052(3)	0.0052(4)	0.0069(4)	0.0095(7)	0.0056(4)
	U_{22}	0.0053(3)	0.0069(2)	0.0086(3)	0.0076(4)	0.0191(6)	0.0203(8)	0.0093(4)
	U_{33}	0.0054(3)	0.0070(2)	0.0094(3)	0.0069(4)	0.0168(5)	0.0129(7)	0.0072(4)
	U_{12}	–0.0004(3)	0.0001(2)	0.0006(2)	–0.0001(4)	0.0024(4)	0.0016(6)	0.0001(3)
	U_{13}	0.0009(3)	0.0014(2)	0.0018(2)	0.0007(4)	0.0030(4)	0.0031(5)	0.0016(3)
	U_{23}	–0.0003(3)	–0.0001(2)	–0.0002(2)	0.0008(4)	–0.0046(5)	–0.0028(6)	0.0000(3)
	U_{eq}	0.0049(2)	0.0063(1)	0.0078(1)	0.0068(2)	0.0143(2)	0.0142(3)	0.0074(2)
O2	x	0.3610(1)	0.36029(8)	0.35929(9)	0.3592(2)	0.3600(1)	0.3609(2)	0.3630(1)
	y	0.2634(1)	0.26139(8)	0.25862(9)	0.2556(2)	0.2554(1)	0.2510(2)	0.2465(1)
	z	0.2935(2)	0.2952(1)	0.2992(2)	0.3033(3)	0.3079(2)	0.3166(3)	0.3237(2)
	U_{11}	0.0076(4)	0.0094(3)	0.0118(4)	0.0107(5)	0.0190(6)	0.0201(8)	0.0122(5)
	U_{22}	0.0052(3)	0.0052(2)	0.0061(3)	0.0064(5)	0.0095(5)	0.0091(6)	0.0068(4)
	U_{33}	0.0084(4)	0.0085(2)	0.0109(3)	0.0125(5)	0.0102(5)	0.0112(6)	0.0096(4)
	U_{12}	–0.0020(3)	–0.0019(2)	–0.0020(2)	–0.0033(4)	–0.0004(4)	–0.0007(6)	0.0029(4)
	U_{13}	0.0022(3)	0.0027(2)	0.0033(2)	0.0031(4)	0.0032(4)	0.0035(6)	0.0019(4)
	U_{23}	–0.0004(3)	–0.0007(2)	–0.0010(2)	–0.0016(4)	–0.0012(4)	–0.0006(5)	–0.0010(3)
	U_{eq}	0.0070(2)	0.0078(1)	0.0096(1)	0.0100(2)	0.0131(2)	0.0136(3)	0.0097(2)
O3	x	0.3536(1)	0.35324(8)	0.35289(8)	0.3526(1)	0.3518(1)	0.3510(2)	0.3502(1)
	y	0.0071(1)	0.00755(8)	0.00802(9)	0.0080(2)	0.0133(1)	0.0160(2)	0.0198(1)
	z	0.0067(2)	0.0075(1)	0.0111(2)	0.0147(3)	0.0013(2)	–0.0016(3)	–0.0066(2)
	U_{11}	0.0059(4)	0.0062(3)	0.0065(4)	0.0066(5)	0.0090(4)	0.0094(6)	0.0067(4)
	U_{22}	0.0083(4)	0.0085(2)	0.0104(3)	0.0103(5)	0.0128(5)	0.0128(6)	0.0100(4)
	U_{33}	0.0059(3)	0.0057(2)	0.0064(3)	0.0063(5)	0.0080(4)	0.0076(6)	0.0070(4)
	U_{12}	0.0006(3)	0.0001(2)	0.0008(2)	0.0000(4)	0.0010(4)	0.0002(5)	–0.0001(3)
	U_{13}	0.0013(3)	0.0019(2)	0.0018(2)	0.0006(4)	0.0033(3)	0.0026(5)	0.0017(3)
	U_{23}	–0.0025(3)	–0.0021(2)	–0.0021(2)	–0.0026(4)	–0.0022(4)	–0.0027(5)	–0.0024(3)
	U_{eq}	0.0065(2)	0.0068(1)	0.0078(1)	0.0080(2)	0.0098(2)	0.0099(3)	0.0079(2)

Note: For pure hedenbergite, an isotropic M2′ split position occupied by 0.01 apfu of Fe^{2+} has been introduced with resulting atomic positions 0, 0.2424, 0.25, and U_{eq} = 0.004(4) (Å^2).

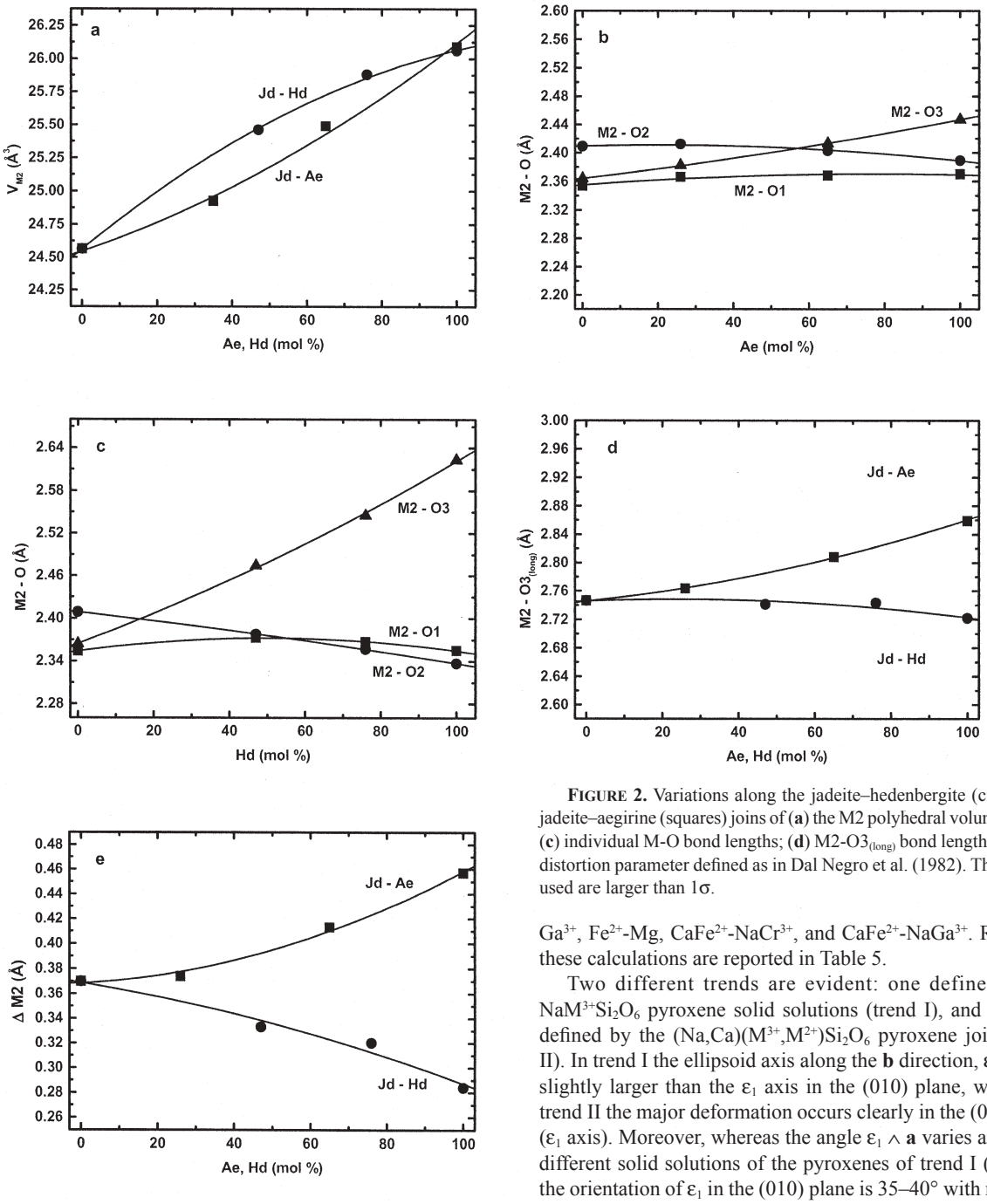

Figure 2. Variations along the jadeite–hedenbergite (circles) and jadeite–aegirine (squares) joins of (**a**) the M2 polyhedral volume; (**b**) and (**c**) individual M-O bond lengths; (**d**) M2-O3$_{(long)}$ bond lengths; (**e**) ΔM2 distortion parameter defined as in Dal Negro et al. (1982). The symbols used are larger than 1σ.

substitutions, the compositional strains were calculated between the end-member jadeite and the samples along the hedenbergite and the aegirine joins. The effect of $NaFe^{3+}$-$CaFe^{2+}$ substitution on the pyroxene structure was characterized by calculating the strain between the end-member aegirine and hedenbergite. For comparison, strain ellipsoids have been calculated also for other pyroxene joins, using the unit-cell parameters of diopside (Di, $CaMgSi_2O_6$, Bruno et al. 1982), kosmochlor (Ks, $NaCrSi_2O_6$, Cameron et al. 1973), and $NaGaSi_2O_6$ pyroxene (NAGA, Nestola et al. 2007), considering therefore the following substitutions: NaAl-CaMg, Al-Cr^{3+}, Al-Ga^{3+}, $NaFe^{3+}$-CaMg, Fe^{3+}-Cr^{3+}, Fe^{3+}-Ga^{3+}, Fe^{2+}-Mg, $CaFe^{2+}$-$NaCr^{3+}$, and $CaFe^{2+}$-$NaGa^{3+}$. Results of these calculations are reported in Table 5.

Two different trends are evident: one defined by the $NaM^{3+}Si_2O_6$ pyroxene solid solutions (trend I), and the other defined by the $(Na,Ca)(M^{3+},M^{2+})Si_2O_6$ pyroxene joins (trend II). In trend I the ellipsoid axis along the **b** direction, ε_2, is only slightly larger than the ε_1 axis in the (010) plane, whereas in trend II the major deformation occurs clearly in the (010) plane (ε_1 axis). Moreover, whereas the angle $\varepsilon_1 \wedge \mathbf{a}$ varies among the different solid solutions of the pyroxenes of trend I (Table 5), the orientation of ε_1 in the (010) plane is 35–40° with respect to **a** (Table 5, Fig. 6) for all joins of trend II. With the exception of $NaM^{3+}Si_2O_6$, ε_1 and ε_3 for pyroxenes of trend I are always much closer to the unit-cell axes **a** and **c** than the ellipsoid axes of the pyroxenes of trend II. This clear change in orientation of the strain ellipsoid is related to the change of coordination of the M2 polyhedron between Na and Ca-pyroxenes. As a consequence of the Ca for Na substitution at the M2 site along the jadeite–hedenbergite and aegirine-hedenbergite joins, the two M2-O3$_{(long)}$ bond lengths slightly decrease whereas the two M2-O3$_{(short)}$ distances significantly increase (Figs. 2c and 2d) so as to give a 4 + 4 coordination. In contrast, along the $NaM^{3+}Si_2O_6$

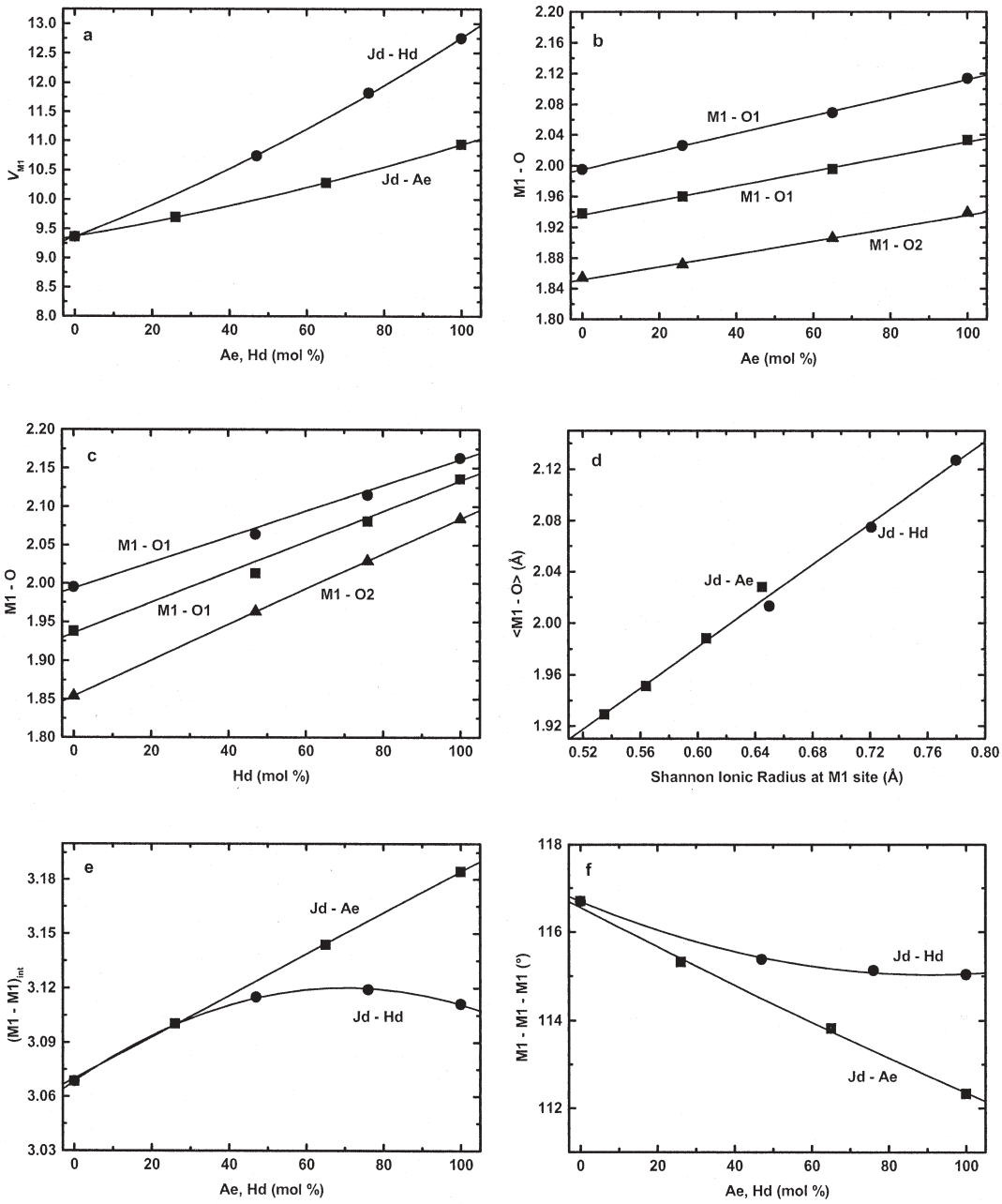

FIGURE 3. Variations along the jadeite–hedenbergite (circles) and jadeite–aegirine (squares) joins of (**a**) the M1 polyhedral volume; (**b**) and (**c**) individual M1-O bond lengths; (**d**) averaged <M1-O> bond lengths; (**e**) M1-M1 intrachain distances; and (**f**) M1-M1-M1 intrachain angle. The symbols used are larger than 1σ.

pyroxene joins, all M2-O3 bond lengths increase in a similar way (e.g., Figs. 2b and 2d) and the 6 + 2 coordination is retained. The different changes in M2-O3 bond lengths affect the O3-O3-O3 kinking angle of the tetrahedral chain with a resulting change in the stacking of the tetrahedral chains and the β angle as shown by Thompson et al. (2005). In both trends, the smallest deformation occurs in the (010) plane close to the **c** axis (ε_3).

Moreover, the change of the **c** axis among pyroxenes of different composition is smaller than that of the other axes and has a limited effect on the overall deformation. In fact, the pyroxene structure cannot freely vary along the **c** axis, which is the direction of elongation of the tetrahedral chains consisting of stiff tetrahedral units. Any expansion or contraction along **c** would require, therefore, significant chain rearrangement. The structural changes that occur along the jadeite–hedenbergite join are, thus, a compromise between counterbalanced effects and result in the observed non-linear change of the **c** axis as a function of composition (Fig. 1c). In fact, whereas Fe^{2+} substitution into the

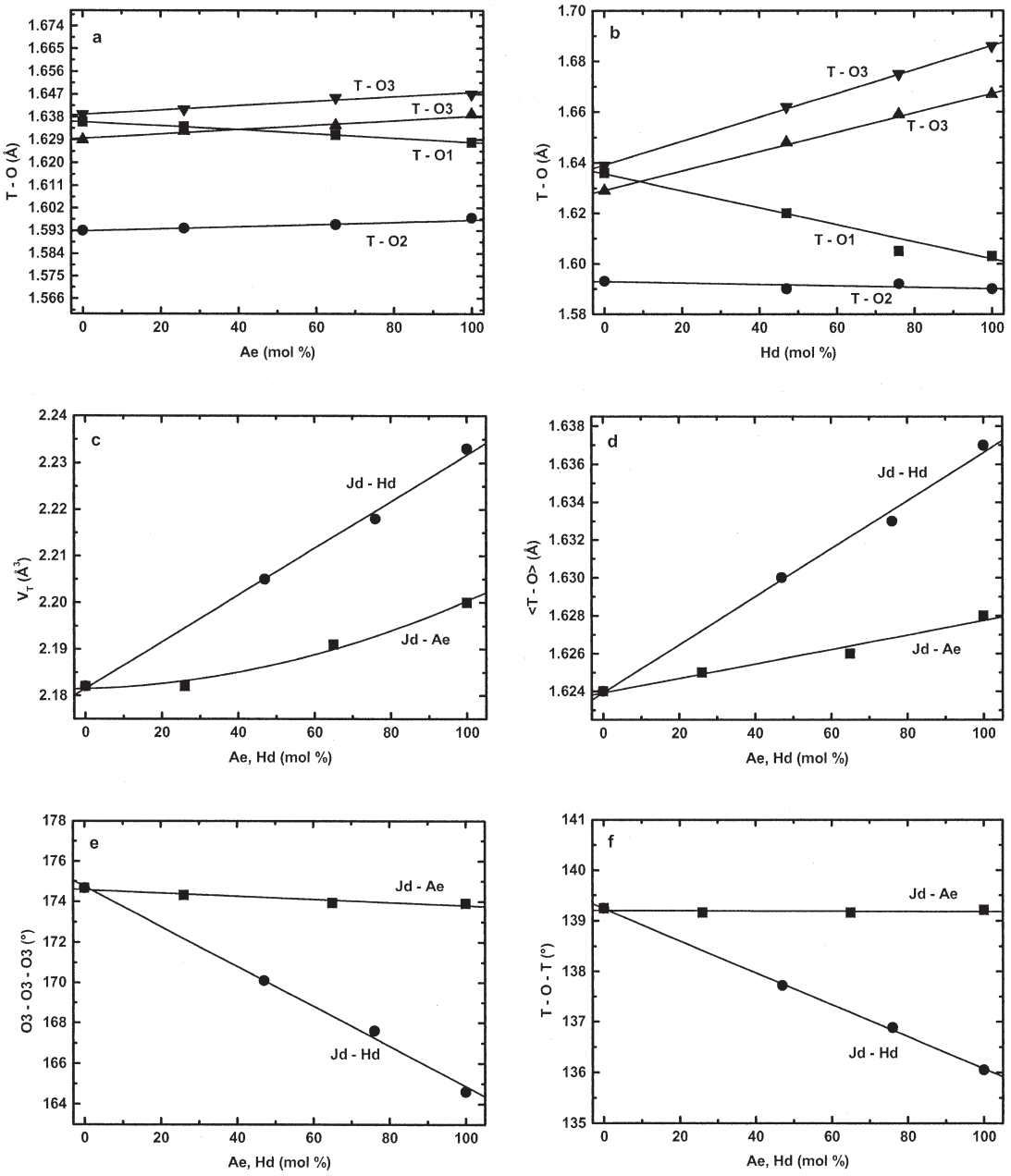

FIGURE 4. Variations along the jadeite–hedenbergite (circles) and jadeite–aegirine (squares) joins of (**a**) and (**b**) individual T-O bond lengths; (**c**) tetrahedral volume; (**d**), O3-O3-O3 angle; and (**e**) T-O-T angle. The symbols used are larger than 1σ.

M1 site of jadeite causes an increase along the **c** axis, as well as along the other axes; the Ca for Na substitution promotes an eightfold coordination for the M2 polyhedron, which is achieved by kinking of the tetrahedral chains and a consequent decrease of the **c** axis. The overall result is a smaller expansion along **c** than that observed along the jadeite–aegirine solid solution. In the latter system, however, the increase of the *c* unit-cell parameter cannot be attributed only to changes in M1 cation sizes (due to the Al/Fe^{3+} substitution), but also to a larger M1-M1 repulsion due to the trivalent cation charge. As shown in Figure 3e, the M1-M1 distances of the M1 polyhedra sharing a common edge increase linearly between jadeite and aegirine. Along the jadeite–hedenbergite system, in which the charge of the M1 cation changes between +3 and +2, the M1-M1 distance increases up to $Jd_{53}Hd_{47}$, similar to that observed in pyroxenes with trivalent M1, and becomes constant at higher hedenbergite contents. This likely is due to the fact that the probability of Al^{3+}-Al^{3+} pairing decreases with increasing hedenbergite content.

LOCAL STRUCTURE

For the O1 and O2 oxygen atoms at intermediate compositions along the Jd–Hd join the structural refinements show a relatively

TABLE 4. Selected bond lengths and angles along the jadeite–aegirine and jadeite–hedenbergite joins investigated in this study

	$Jd_{100}Hd_0$	$Jd_{74}Ae_{26}$	$Jd_{35}Ae_{65}$	Jd_0Ae_{100}	$Jd_{53}Hd_{47}$	$Jd_{24}Hd_{76}$	Jd_0Hd_{100}
M2-O1 (Å)	2.354(1)×2	2.3641(8)×2	2.3659(9)×2	2.369(2)×2	2.372(1)×2	2.368(2)×2	2.357(1)×2
M2-O2 (Å)	2.409(1)×2	2.4098(7)×2	2.4004(8)×2	2.388(2)×2	2.381(1)×2	2.357(2)×2	2.336(1)×2
M2-O3 (Å)	2.364(1)×2	2.3801(8)×2	2.411(1)×2	2.446(2)×2	2.477(1)×2	2.545(2)×2	2.624(1)×2
M2-O3 (Å)	2.746(1)×2	2.7605(8)×2	2.8056(9)×2	2.857(2)×2	2.742(1)×2	2.742(2)×2	2.722(1)×2
<M2-O>	2.468	2.479	2.496	2.515	2.493	2.503	2.510
V (Å^3)	24.621(20)	25.000(15)	25.490(23)	26.122 (35)	25.525(21)	25.937(37)	26.060(28)
M1-O1 (Å)	1.938(1)×2	1.9579(7)×2	1.9933(8)×2	2.031(1)×2	2.015(1)×2	2.080(2)×2	2.135(1)×2
M1-O1 (Å)	1.995(1)×2	2.0243(7)×2	2.0673(8)×2	2.113(1)×2	2.068(1)×2	2.116(2)×2	2.162(1)×2
M1-O2 (Å)	1.854(1)×2	1.8699(7)×2	1.9046(8)×2	1.939(2)×2	1.964(1)×2	2.029(2)×2	2.084(1)×2
<M1-O>	1.929	1.951	1.988	2.028	2.016	2.075	2.127
V (Å^3)	9.383(9)	9.723(6)	10.280(10)	10.941 (17)	10.779(11)	11.847(18)	12.754(14)
T-O1 (Å)	1.636(1)	1.6326(7)	1.6295(9)	1.628(1)	1.620(1)	1.604(2)	1.602(1)
T-O2 (Å)	1.593(1)	1.5926(7)	1.5940(8)	1.598(2)	1.591(1)	1.592(2)	1.589(1)
T-O3 (Å)	1.629(1)	1.6307(8)	1.6331(8)	1.638(1)	1.648(1)	1.661(2)	1.667(1)
T-O3 (Å)	1.639(1)	1.6392(7)	1.6440(8)	1.646(1)	1.664(1)	1.674(2)	1.687(1)
<T-O>	1.624	1.624	1.625	1.628	1.631	1.633	1.636
V (Å^3)	2.184(3)	2.188(2)	2.191(3)	2.203 (5)	2.210(3)	2.221(6)	2.233(4)
O3-O3-O3 (°)	174.67(9)	174.32(6)	173.94(7)	173.89(13)	169.9(1)	167.6(1)	164.6(1)
T-O-T (°)	139.24(7)	139.15(5)	139.16(7)	139.21(8)	137.68(7)	136.88(7)	136.05(8)
M1-M1-M1 (°)	116.70(4)	115.32(2)	113.83(1)	112.76(2)	115.34(4)	115.13(4)	115.04(3)
M1-M1 (Å)	3.0680(7)	3.1006(3)	3.1435(3)	3.1844(4)	3.1158(5)	3.1193(5)	3.1114(4)

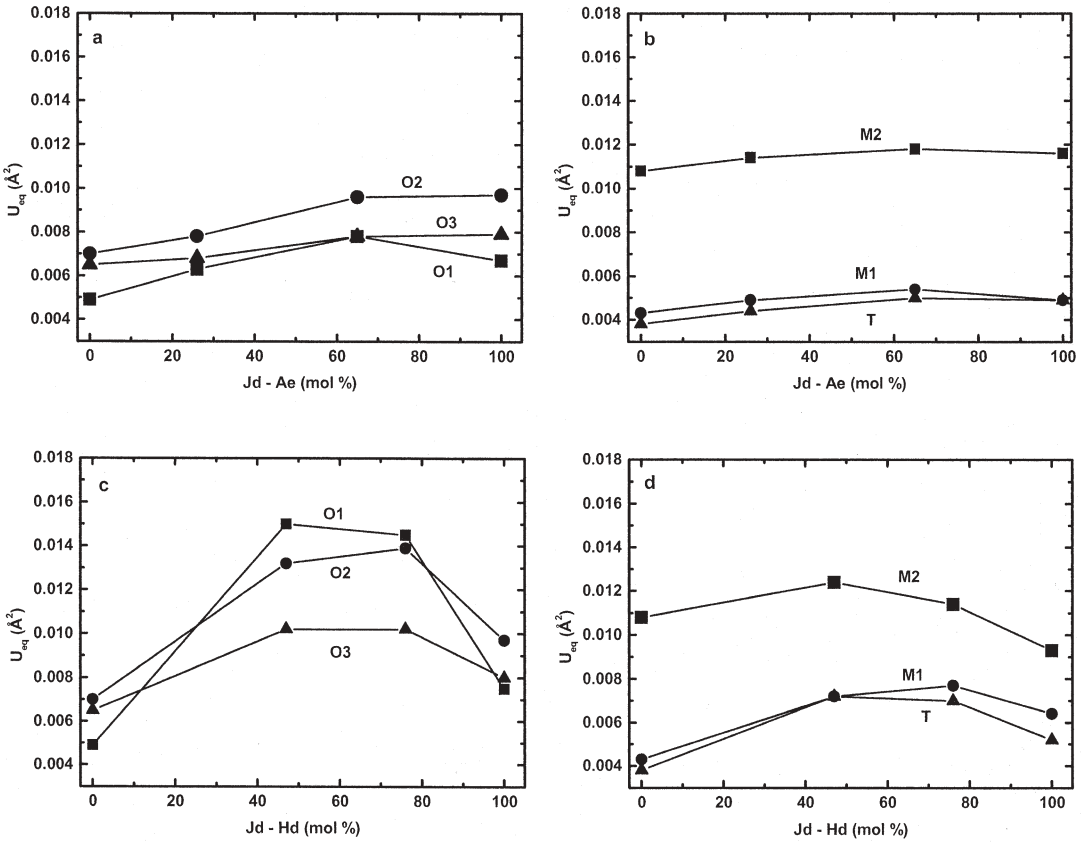

FIGURE 5. Variation with composition of the equivalent displacement parameter U_{eq} (**a**) and (**b**) for jadeite–aegirine; (**c**) and (**d**) for jadeite–hedenbergite. The symbols used are larger than 1σ.

large displacement ellipsoid with respect to those obtained for all other samples. This may indicate positional disorder, due likely to the coexistence of different local structural configurations. In the average structure, obtained from the X-ray structural refinements, local configurations cannot be resolved and are usually averaged giving rise to large displacement parameters. Local structural configurations arise in solid solutions due to the different local environment of substituting cations and may be described as site splitting, giving the structural position of subsites. These subsites are often overlooked, as they are very close to the averaged site position and often below the resolution of the measurements. Site splitting in clinopyroxenes and orthopyroxenes (Rossi et

TABLE 5. Magnitude and orientation of the strain ellipsoid in different clinopyroxenes

Cpx	Strain (× 10^{-3})			Angle with **a** (toward **c**)				
	ε_1	ε_2	ε_3	ε_1	ε_2	ε_3	β (°)	Δβ (°)
Jd-$Jd_{53}Hd_{47}$	25.7	24.3	5.4	37	90	127	107.624–106.725	0.90
Jd-$Jd_{24}Hd_{76}$	45.5	40.3	4.4	35	90	125	107.624–105.904	1.72
Jd-Hd	65.1	53.5	–1.3	35	90	125	107.624–104.862	2.76
Jd-$Jd_{74}Ae_{26}$	5.7	6.2	3.6	24	90	114	107.624–107.624	0.06
Jd-$Jd_{35}Ae_{65}$	14.9	16.2	8.9	11	90	111	107.624–107.600	0.02
Jd-Ae	25.3	27.4	13.1	11	90	111	107.624–107.579	0.04
Ae-Hd	41.1	25.4	–16.5	40	90	130	107.579–104.862	2.72
Jd-Di	48.7	39.9	0.6	35	90	125	107.624–105.620	2.00
Jd-Ks	17.6	18.3	7.7	23	90	113	107.624–107.370	0.25
Jd-NAGA	13.4	15.5	7.9	8	90	98	107.624–107.629	0.00
Ae-Di	25.2	11.2	–14.7	40	90	130	107.579–105.620	1.96
Ks-Ae	9.1	8.9	3.9	–16	90	75	107.370–107.579	–0.21
NAGA-Ae	11.8	11.7	5.1	13	90	113	107.629–107.579	0.05
Di-Hd	15.7	14.0	–1.8	35	90	125	105.620–104.862	0.76
Ks-Hd	47.2	34.6	–9.4	37	90	127	107.370–104.862	2.51
NAGA-Hd	52.1	37.4	–10.3	37	90	127	107.629–104.862	2.77

Notes: The seven compositions studied in this work were compared with diopside ($CaMgSi_2O_6$, Bruno et al. 1982), kosmochlor (Ks, $NaCrSi_2O_6$, Cameron et al. 1973) and $NaGaSi_2O_6$ (NAGA, Nestola et al. 2007) *C*2/*c* pyroxenes. ε_2 has been chosen as the ellipsoid axis parallel to the **b**-axis. Jadeite, aegirine, and hedenbergite data = this work; diopside = Bruno et al. (1982); kosmochlor = Cameron et al. (1973); $NaGaSi_2O_6$ = Nestola et al. (2007).

al. 1987; Boffa Ballaran et al. 1998; Nestola and Tribaudino 2003) was found for the M2 site (M2-M2' splitting), but also for O atoms (Tribaudino et al. 1989; Tribaudino and Nestola 2002). Substitution of Na + Al for Ca + Fe^{2+} along the join jadeite–hedenbergite is likely to promote the presence of local jadeite-like and hedenbergite-like configurations, due to next nearest neighbor interaction related to the requirement of local charge balance. The larger displacement parameter of the O1 and O2 oxygen atoms for $Jd_{53}Hd_{47}$ and $Jd_{24}Hd_{76}$ suggests, therefore, the presence of site splitting at these two structural sites.

ACKNOWLEDGMENTS

F. Nestola thanks the Alexander von Humboldt Foundation for financing this research. Fernando Camara is thanked for his scientific discussions, Raul Carampin for collecting electron microprobe data and Hubert Schulze and Leonardo Tauro for preparing single-crystal thin sections for microprobe analyses. C.L. was supported by the Swiss National Science Foundation (SNF grant 200020-111725/1 to M.W. Schmidt). The authors thank R. Thompson, L. Bindi, and D. Gatta for their reviews that strongly improved this manuscript. This study was financed by the Alexander von Humboldt Foundation.

REFERENCES CITED

Angel, R.J. (2003) Automated profileanalysis for single-crystal diffraction data. Journal of Applied Crystallography, 36, 295–300.

——— (2004) Absorption corrections for diamond-anvil cells implemented in the software package Absorb 6.0. Journal of Applied Crystallography, 37, 486–492.

Boffa Ballaran, T., Carpenter, M., Domeneghetti, M.C., and Tazzoli, V. (1998) Structural mechanisms of solid solution and cation ordering in augite-jadeite pyroxenes: I. A macroscopic perspective. American Mineralogist, 83, 419–433.

Bruno, E., Carbonin, S., and Molin, G.M. (1982) Crystal structures of Ca-rich clinopyroxenes in the $CaMgSi_2O_6$–$Mg_2Si_2O_6$ join. Tschermacks Mineralogische und Petrographische Mitteilungen, 29, 223–240.

Cameron, M., Sueno, S., Prewitt, C.T., and Papike, J.J. (1973) High temperature crystal chemistry of acmite, diopside, hedenbergite, jadeite, spodumene, and ureyite. American Mineralogist, 58, 594–618.

Carpenter, M.A., Domeneghetti, M.C., and Tazzoli, T. (1990a) Application of Landau theory to cation ordering in omphacite I: Equilibrium behavior. European Journal of Mineralogy, 2, 7–18.

——— (1990b) Application of Landau theory to cation ordering in omphacite II: Kinetic behavior. European Journal of Mineralogy, 2, 19–28.

Dal Negro, A., Carbonin, S., Molin, G., Cundari, A., and Piccirillo, E.M. (1982) Intracrystalline cation distribution in natural clinopyroxenes of tholeiitic, transitional and alkaline basaltic rocks. In S.K. Saxena, Ed., Advances in Physical Geochemistry, 2, p. 117–150. Springer-Verlag, New York.

Gasparik, T. (1985) Experimental determined compositions of diopside-jadeite pyroxene in equilibrium with albite and quartz at 1200–1350 °C and 15–34 kbar. Geochimica et Cosmochimica Acta, 49, 865–870.

Heuer, M., Huber, A.L., Bromiley, G.D., Fehr, K.T., and Bente, K. (2005) Characterization of synthetic hedenbergite ($CaFeSi_2O_6$)-petedunnite ($CaZnSi_2O_6$) solid solution series by X-ray single crystal diffraction. Physics and Chemistry of Minerals, 32, 552–563.

Holland, T.J.B. (1983) The experimental determination of activities in disordered and shortrange ordered jadeitic pyroxenes. Contributions to Mineralogy and Petrology, 82, 214–220.

Ibers, J.A. and Hamilton, W.C., Eds. (1974) International Tables for X-ray Crystallography, IV, p. 99–101. Kynoch Press, Birmingham, U.K.

Liu, J. and Bohlen, R. (1995) Mixing properties and stability of jadeite-acmite pyroxene in the presence of albite and quartz. Contributions to Mineralogy and Petrology, 119, 433–440.

Nestola, F. and Tribaudino, M. (2003) The structure of *Pbca* orthopyroxenes along the join diopside–enstatite ($CaMgSi_2O_6$–$Mg_2Si_2O_6$). European Journal of Mineralogy, 15, 365–371.

Nestola, F., Boffa Ballaran, T., Liebske, C., Bruno, M., and Tribaudino, M. (2006) High-pressure behavior along the jadeite $NaAlSi_2O_6$–aegirine $NaFeSi_2O_6$ solid solution up to 10 GPa. Physics and Chemistry of Minerals, 33, 417–425.

Nestola, F., Rotiroti, N., Bruno, M., Tribaudino, M., van Smaalen, S., Ohashi, H., and Redhammer, G. (2007) Low-temperature behavior of $NaGaSi_2O_6$. American Mineralogist, 92, 560–569.

Oberti, R. and Caporuscio, F.A. (1991) Crystal chemistry of clinopyroxenes from mantle eclogites: a study of the key role of the M2 site population by means of crystal-structure refinement. American Mineralogist, 76, 1141–1152.

Ohashi, Y. and Burnham, C.W. (1973) Clinopyroxene lattice deformations: the roles of chemical substitution and temperature. American Mineralogist, 58, 843–849.

Popp, R.K. and Gilbert, M.C. (1972) Stability of acmite-jadeite pyroxenes at low pressure. American Mineralogist, 51, 1210–1231.

Redhammer, G.J., Amthauer, G., Lottermoser, W., and Treutmann, W. (2000) Synthesis and structural properties of clinopyroxenes of the hedenbergite $CaFe^{2+}Si_2O_6$–aegirine $NaFe^{3+}Si_2O_6$ solid-solution series. European Journal of Mineralogy, 12, 105–120.

Redhammer, G.J., Amthauer, G., Roth, G., Tippelt, G., and Lottermoser, W. (2006) Single crystal X-ray diffraction and temperature dependent ^{57}Fe Mössbauer spectroscopy on the hedenbergite–aegirine $(Ca,Na)(Fe^{2+},Fe^{3+})Si_2O_6$ solid solution. American Mineralogist, 91, 1271–1292.

Rossi, G., Smith, D.C., Ungaretti, L., and Domeneghetti, M.C. (1983) Crystal-chemistry and cation ordering in the system diopside-jadeite: a detailed study by crystal structure refinement. Contributions to Mineralogy and Petrology, 83, 247–258.

Rossi, G., Oberti, R., Dal Negro, A., Molin, G.M., and Mellini, M. (1987) Residual electron density at the M2 site in *C*2/*c* clinopyroxenes: relationships with bulk chemistry and sub-solidus evolution. Physics and Chemistry of Minerals, 14, 514–520.

Shannon, R.D. (1976) Revised effective ionic radii and systematic studies of interatomic distances in halides and chalcogenides. Acta Crystallographica, A32, 751–767.

Sheldrick, G.M. (1997) SHELX, programs for Crystal Structure Analysis (Release 97-2). Institüt für Anorganische Chemie der Universität, Tammanstrasse 4, D-3400 Göttingen, Germany.

Thompson, R.M. and Downs, R.T. (2004) Model pyroxenes II: structural variation as a function of tetrahedral rotation. American Mineralogist, 89, 614–628.

Thompson, R.M., Downs, R.T., and Redhammer, G.J. (2005) Model pyroxenes III: volume of *C*2/*c* pyroxenes at mantle *P*, *T*, and *X*. American Mineralogist, 90, 1840–1851.

Tribaudino, M. and Nestola, F. (2002) Average and local structure in $P2_1/c$ clinopyroxenes along the join diopside–enstatite ($CaMgSi_2O_6$–$Mg_2Si_2O_6$). European Journal of Mineralogy, 14, 549–555.

Tribaudino, M., Benna, P., and Bruno, E. (1989) Average structure and M2 site configurations in *C*2/*c* clinopyroxenes along the Di–En join. Contributions to Mineralogy and Petrology, 103, 452–456.

Tutti, F., Dubrovinsky, L., and Saxena, S.K. (2000) High pressure phase transformation of jadeite and stability of $NaAlSiO_4$ with calcium-ferrite type structure in the lower mantle conditions. Geophysical Research Letters, 27, 2025–2028.

MANUSCRIPT RECEIVED DECEMBER 18, 2006
MANUSCRIPT ACCEPTED MARCH 26, 2007
MANUSCRIPT HANDLED BY G. DIEGO GATTA